



Morphological description of desiccation cracks in soils: insights from the perspective of anisotropy

Bei-Bing Dai^{1,2} · Jun Yang³ · Feng-Tao Liu⁴ · Chao-Sheng Tang⁵ · Tian-Qi Li¹

Received: 22 March 2021 / Accepted: 2 February 2022 / Published online: 11 February 2022
© Springer-Verlag GmbH Germany, part of Springer Nature 2022

Abstract

The characterization of a soil crack network requires a comprehensive understanding of statistics and has been of longstanding interest but not well resolved. By performing a series of desiccation cracking tests with a soil mixture comprising fines and montmorillonite, we make a systematic examination of the effect of the container shape on the anisotropic distribution of a crack network. The statistical analyses show that the angular distributions of crack orientation and length vectors in the cases of square and rectangular shapes have the feature of orthogonal concentration in two angular zones near the horizontal and vertical directions (i.e., $-15^\circ < \phi < 15^\circ$ and $75^\circ < \phi < 105^\circ$) and that a larger magnitude of anisotropy results in a more intense concentration around the principal direction of anisotropy, whereas the angular distributions of these two vectors are in an almost isotropic state for the circular shape. The angular distributions of crack width and area vectors do not have an orthogonal concentration for any container shape. The distributions of crack area vectors approximate to an isotropic state for the square and circular shapes and have weak anisotropy for the rectangular shapes, with the principal direction of anisotropy being near the vertical direction. It is revealed that either the crack length or width vector exercises a dominant influence on the angular distribution anisotropy of crack area vectors only if its angular distribution bears relatively strong anisotropy.

Keywords Soil layer · Desiccation cracking · Morphological description · Anisotropy · Container shape · Vector quantity

Introduction

It is a widely observed phenomenon that soils suffer from shrinkage-induced cracking in a desiccating environment that is driven by thermal variation, solar radiation, and air circulation (Kindle 1917; Bai et al. 2000; Tay et al. 2001; Krisdani et al. 2008; Li and Zhang 2011; Fernandes et al. 2015; Tollenaar et al. 2017; Julina and Thyagaraj 2020). Cracking also occurs for many other

natural/artificial brittle/ductile materials (e.g., concrete, rock, steel, and paper), given a particular external or internal condition (Baker 1981; Omidi et al. 1996; Nishiuma and Miyazima 1999; Alava et al. 2006; Cortet et al. 2008; Zhao et al. 2016; Kokkonniemi et al. 2017; Boehm-Couriault et al. 2020). In soil, the presence of cracks strongly affects the hydraulic and mechanical properties, in that cracks in soil offer preferential pathways for water infiltration, and they may also act as potential slipping planes and undermine the integrity and strength of the soil. Soil cracking is thus thought to affect the stability and serviceability of infrastructure such as foundations and embankments and sometimes cause infrastructure failure (Baker 1981; Omidi et al. 1996; Hawkins 2013; Khan et al. 2017; Bulolo et al. 2021). Meanwhile, cracks serve as main channels for gas evaporation and solute transfer in soil and affect the physical and chemical properties of the soil. Cracking also leads to the erosion of soils, damage to botanical roots, and reductions in crop yields (Tang et al. 2018; Wang et al. 2018). Soil cracking is therefore an important and fascinating phenomenon, and it has been studied extensively given its implications in agriculture and engineering.

✉ Feng-Tao Liu
celiuft@glut.edu.cn

¹ School of Civil Engineering, Sun Yat-Sen University, Guangzhou, China

² Southern Marine Science and Engineering Guangdong Laboratory (Zhuhai), Zhuhai, China

³ Department of Civil Engineering, The University of Hong Kong, Hong Kong, China

⁴ College of Civil Engineering and Architecture, Guilin University of Technology, Guilin, China

⁵ School of Earth Sciences and Engineering, Nanjing University, Nanjing, China

Of primary concern to researchers is the characterization of the morphology of the crack network, as the pattern of the geometrical distribution of cracks is closely interrelated to the overall physical and mechanical states of the soil mass. Centering around the morphological description of the crack network, researchers have experimentally, numerically, and analytically analyzed the effects of various factors (e.g., the layer thickness, drying rate, soil type, boundary condition, and temperature) on crack initiation, propagation, and termination and on the morphological features of the overall network (Kindle 1917; Miller et al. 1998; Weiberger 1999; Bai et al. 2000; Bohn et al. 2005a; Rodríguez et al. 2007; Tang et al. 2008; Péron et al. 2009; Goehring et al. 2010; Costa et al. 2013; Liu et al. 2013; Sánchez et al. 2014; Stirling 2014; Khatun et al. 2015; Zhang et al. 2016; Sun and Cui 2017; Tollenaar et al. 2017; Lakshmikantha et al. 2018; Wang et al. 2018; Tang et al. 2019; Vo et al. 2019; Zeng et al. 2019; An et al. 2020; Cheng et al. 2020; Yuan et al. 2021). It is recognized that cracks form in a sequential manner and a secondary (later) crack in general intersects a primary (earlier) crack at a right angle to generate a T-junction or at 120° to generate a Y-junction, such that the entire crack network is made up of interconnected fractures that are organized in polygonal shapes (Weinberger 1999; Bohn et al. 2005a; Goehring et al. 2010; Goehring 2013). Interestingly, with the processed crack images, several researchers have investigated the hierarchical structure of fractures and used temporal and geometrical trees to graphically trace the process of crack formation and describe the morphological characteristics of the eventual crack pattern (Bohn et al. 2005a; 2005b; Modes et al. 2016). Other researchers, such as Sánchez et al. (2014) and Gui and Zhao (2015), have developed continuum or discontinuum models that mimic through numerical means the crack formation process and reproduce the morphology of desiccation cracks.

To obtain a more appropriate quantitative morphology characterization of the crack network, researchers have conducted fractal and statistical analyses of basic geometrical features (e.g., the crack length, crack width, and crack area) and proposed several descriptive indices along with probability density functions. The descriptive indices include the crack ratio, crack length density, mean or maximum crack width, variation gradient of the crack ratio, crack intensity factor, crack reduction factor, and similarity index (Li and Zhang 2011; Tang et al. 2011; Liu et al. 2013; Zhang et al. 2013; Arena et al. 2014; DeCarlo and Shokri 2014; Peng et al. 2016; Wang et al. 2017; Lakshmikantha et al. 2018; Basson and Ayothiraman 2020), and the density distribution functions are mainly built with respect to basic geometrical parameters, such as the crack length and width (Tang et al. 2011). It has been shown in the literature that these indices and functions, to some extent, describe the morphological features of the crack network and quantify

the effects of various external and internal factors. It is additionally noted that such descriptive indices and functions are defined on the basis of scalar quantities, such as the crack length and width, and they are thus treated as scalar parameters and functions.

However, anisotropy is an important morphological feature of the crack network as observed in nature and laboratory experiments. Figure 1a shows the development of cracks in a preferential direction on outdoor bare ground, which is presumably associated with the ground surface characteristics created by the directional flow of rainwater. Additionally, it has been found in experiments that a memory of vibration and flow direction can be imprinted on the morphology of the eventual crack network of a desiccating paste and this memory effect is responsible for an anisotropic configuration of desiccation cracks (see Fig. 1b) (Nakahara and Matsuo 2006a, b; Matsuo and Nakahara 2012; Nakayama et al. 2013; Kitsunozaki et al. 2016; 2017; Nakahara et al. 2019; Akiba and Shima 2019). Khatun et al. (2013) conducted an experimental study on the cracking behavior of a synthetic clay gel and found that the crack formation displayed the signature (i.e., the memory) of an electric field enforced during the drying process. Lakshmikantha et al. (2018) performed desiccation cracking tests using soil specimens with various shapes and sizes and observed an anisotropic crack pattern. Moreover, with the development of a phase-field model of a cohesive fracture with frictionless contact and random fracture properties, Hu et al. (2020) reproduced through finite element simulations the anisotropic pattern of soil cracks and the memory effect (i.e., a memory of the agitation mode) observed in the experiments.

The anisotropic distribution of cracks (e.g., crack orientations and lengths) gives rise to the anisotropic hydraulic conductivity for soil masses; i.e., the hydraulic conductivity is direction dependent. As a result, the water infiltration rate is also direction-dependent owing to the anisotropic hydraulic conductivity. This situation may be encountered in the recharge of a dried pond, the boundaries of which have a

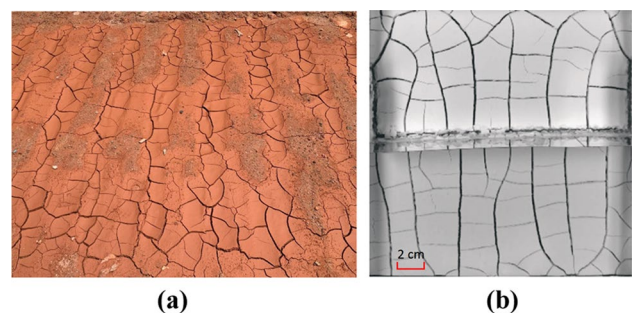


Fig. 1 **a** Development of cracks in a preferential direction on bare ground at the campus of Sun Yat-sen University and **b** the anisotropic feature of a crack network observed in laboratory tests (from Nakahara and Matsuo 2006b)

particular geometrical shape (e.g., a rectangle or square). In addition, the presence of cracks weakens the integrity of soil masses, and cracks can serve as part of slip surfaces that have little or even no shear strength (Li and Zhang 2011; Sánchez et al. 2014). The anisotropic distribution of cracks thus makes the mobilization of the shear strength of soil masses different in various directions. The anisotropic mobilization of the shear strength tends to make soil masses fail along the direction where the cracks concentrate. With the above concerns, it is naturally important to characterize and understand the anisotropic cracking pattern of desiccating soils.

It is apparent that the anisotropic crack morphology is linked with the directional distribution of a certain vector quantity. It thus seems to be a great challenge to describe the anisotropic feature of crack morphology with previous scalar parameters and functions. The present paper deals principally with the morphological description of the crack network from the perspective of anisotropy; to the best of the authors' knowledge, few studies have quantitatively interpreted the anisotropic properties of the soil crack network. To this end, a number of vector quantities, together with several scalar quantities, are firstly introduced on the basis of crack information that includes both the crack orientation and crack magnitude (e.g., the crack length and crack width). A series of desiccation cracking tests, in which five container shapes are considered, are then undertaken with a soil mixture comprising fines and montmorillonite. The morphology of desiccation cracks is described by a statistical analysis of scalar and vector data of the cracks, which are

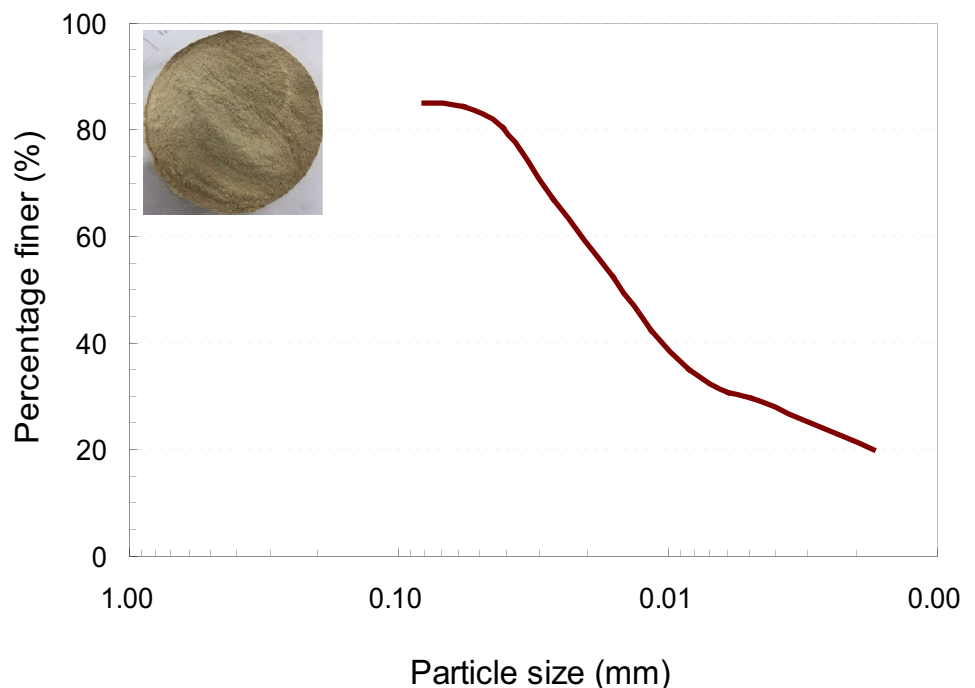
acquired through image analysis with the software Crack Image Analysis System (CIAS, Tang et al. (2008), available at www.climate-engeo.com). Furthermore, a comparative analysis of the effect of the container shape on the anisotropic feature of the crack network is conducted. It is hoped that the results reported in this study will improve our understanding of the soil crack network morphology from the perspective of anisotropy.

Test setup and procedure

The soil for testing is a mixture (see the inset in Fig. 2) of fines sourced from a local sandy soil and montmorillonite. The montmorillonite accounts for 40% of the mixture by weight. The fines were sieved out from completely decomposed granite soil and had a particle diameter less than 0.075 mm. The curve of the overall particle size distribution is given in Fig. 2, with the mean particle size d_{50} being 0.015 mm. The specific weight of soil grains ranges from 2.65 to 2.70 g/cm³. The liquid limit and plastic limit of the soil mixture were measured to be 78.5% and 33.8%. There was typically an obvious upper layer of water segregating from the lower solid phase when the slurry prepared for the cracking test settled and soil particles deposited thoroughly, and it is supposed that the water content of the slurry in the initial state is far higher than that at the liquid limit (i.e., 78.5%).

Containers made of transparent acrylic plates were used to hold the soil slurry for the cracking test and had an area of approximately 1200 cm². Five container shapes

Fig. 2 Particle size distribution of the soil mixture used in this study



were considered in the experimental study, including the square shape (34.6 cm × 34.6 cm), circular shape (39.1 cm in diameter), and three rectangular shapes with aspect ratios of AR = 1:2 (24.5 cm × 49 cm), 1:3 (20 cm × 60 cm), and 1:4 (17.3 cm × 69.2 cm). We adopted the ratio between the width and length to define the aspect ratio of a rectangle as tacitly used by other researchers in describing regular geometrical shapes such as rectangles (Lakshmikantha et al. 2018; Sánchez et al. 2014).

The desiccation cracking tests were performed in a room with the temperature controlled at 25 ± 2 °C by an air conditioner. To reliably analyze the anisotropy of the cracking pattern, we performed four sets of parallel tests and combined the four sets of data in an overall data analysis. Note that it is difficult to superimpose error bars in the diagrams of directional data for error analysis. The thickness of the dry soil layers was 2.8 ± 0.2 mm. The soil volume was basically the same for the different containers because the thickness of the soil layer, as well as the container area (1200 cm²), was almost the same, and the effect of the soil volume was thereby eliminated for a comparative analysis of the effect of the container shape.

The interface between the soil and container bottom plays an important role in determining the soil cracking behavior (DeCarlo and Shokri 2014; Liu et al. 2016; Lakshmikantha et al. 2018; Zeng et al. 2019). Despite this, the effect of the interface condition is not the focus of the present study. The

interface friction condition was ensured to be the same in all the tests, and we did not specially roughen or smoothen the bottom of the containers. The interface contact behavior between the soil and container bottom is assumed to depend on the original properties of the two substances in contact.

Upon the completion of the cracking of soil layers, the specimens were moved with caution into a mini-studio for photography (see Fig. 3). Photographs of soil cracks were processed using the software CIAS; examples are shown in Fig. 4. The crack data in terms of the crack position, length, width, and area were extracted by CIAS from the processed images and used to further analyze and characterize the morphology of the crack network. The orientation of a crack was determined from the coordinates of the start and end points of the crack.

Methodology of the analysis of the crack pattern and anisotropy

The length, width, and area of a given crack are the essential elements of crack morphology. For a sound description of the crack network, the cumulative distribution curves of such elements (i.e., the crack length, width, and area), which are comparable to the particle size distribution curve in soil mechanics, are identified by a statistical analysis of the relative data obtained from the image analysis. Two indices are

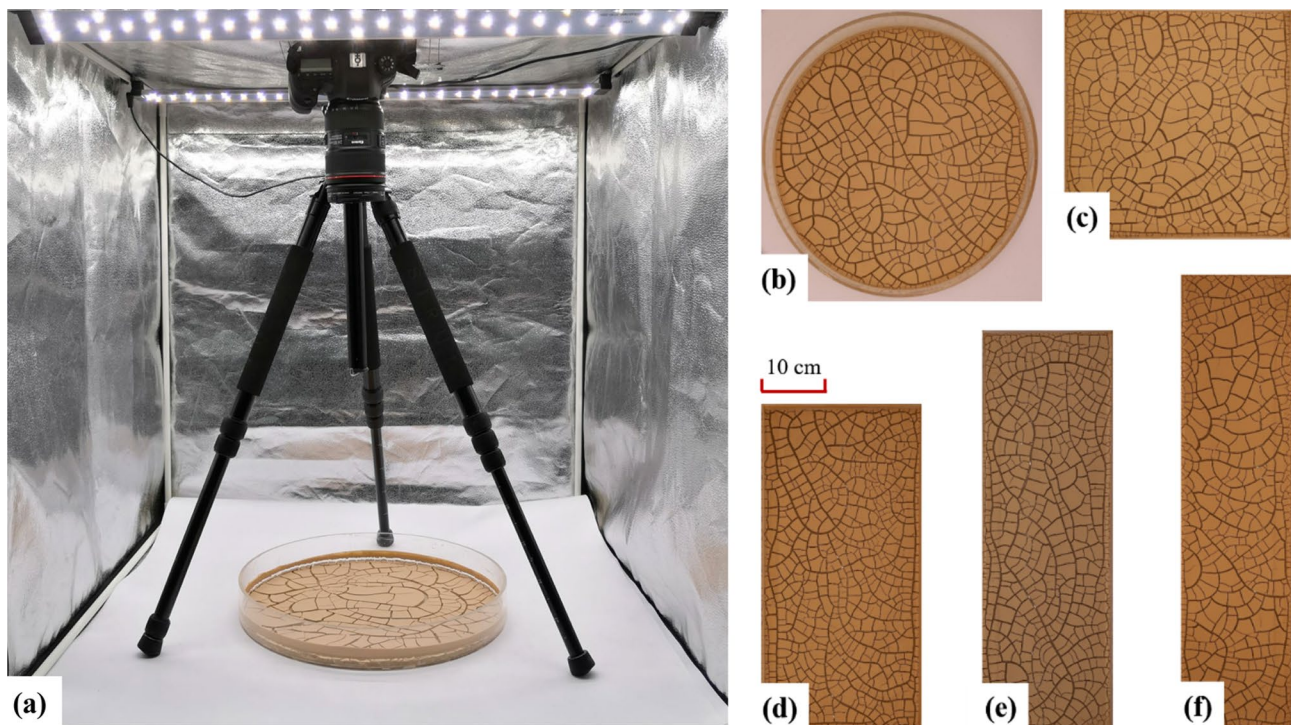


Fig. 3 Images of **a** the photography equipment and cracks in containers having **b** a circular shape and rectangular shapes with **c** AR = 1:1, **d** AR = 1:2, **e** AR = 1:3, and **f** AR = 1:4

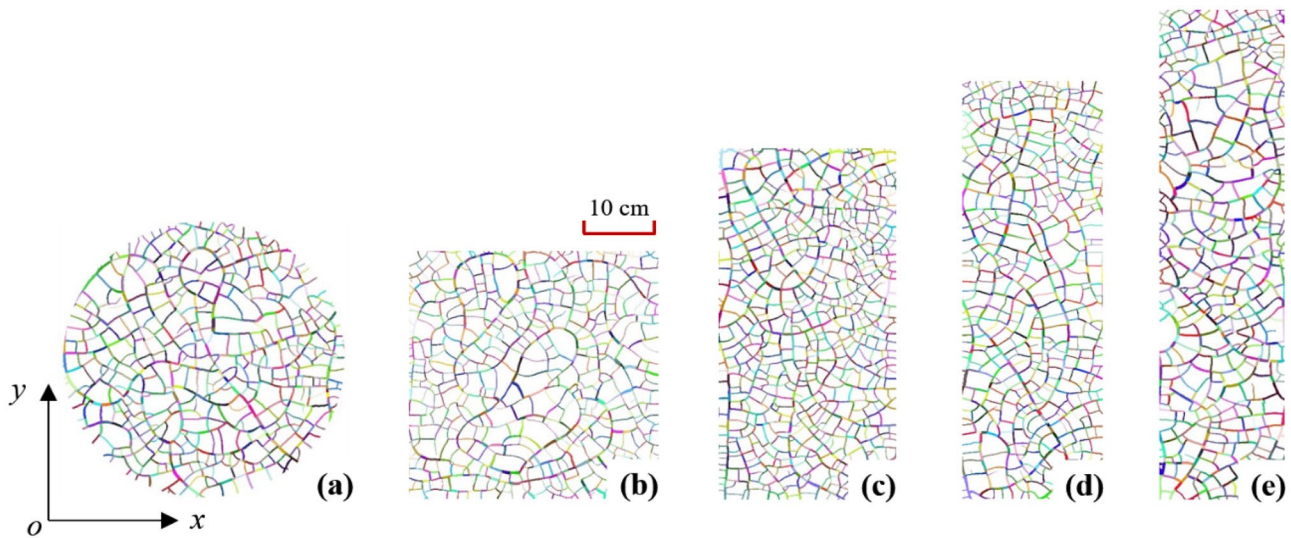


Fig. 4 Processed images of the cracks in containers having **a** a circular shape and rectangular shapes with **b** AR=1: 1, **c** AR=1:2, **d** AR=1:3, and **e** AR=1:4

then used to further characterize these distribution curves: the median index (i.e., l_{50} for the crack length, w_{50} for the crack width, and s_{50} for the crack area) and the coefficient of uniformity (i.e., C_{ul} for the crack length, C_{uw} for the crack width, and C_{us} for the crack area). We take the crack length as an example. As seen in Fig. 5, l_{50} represents the crack length, with cracks shorter than this value accounting for 50% of all cracks by number. C_{ul} is defined as the ratio of l_{60} over l_{10} (i.e., $C_{ul} = l_{60}/l_{10}$), wherein l_{60} and l_{10} have physical meanings similar to that of l_{50} and the only difference is the value of the cumulative percentage. The indices of w_{50} and s_{50} are determined in a manner analogous to that adopted for l_{50} , and the definitions of C_{uw} and C_{us} are comparable to the definition of C_{ul} .

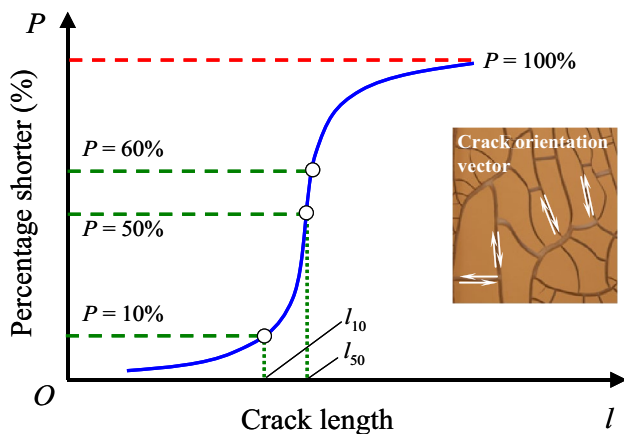
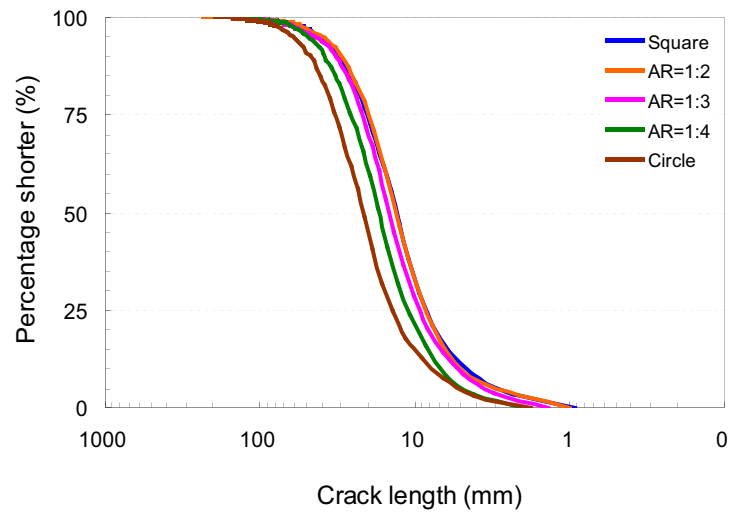


Fig. 5 Schematic illustrations of the definitions of scalar and vector quantities

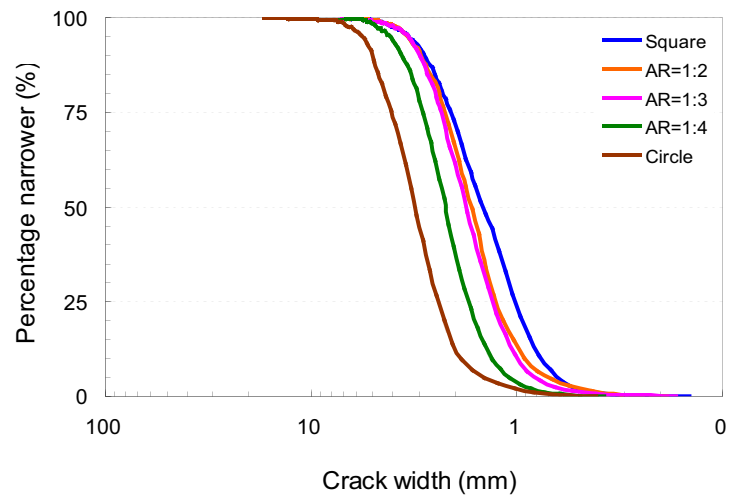
In addition to the scalar quantities introduced above, a number of vector quantities are proposed in current study to describe the morphology of the crack network. As indicated by the inset of Fig. 5, the orientation of a crack is treated as a directional vector for an examination of the morphological characteristics of the crack network, and a statistical analysis is then conducted with respect to the crack orientation vectors to find their angular distribution pattern. Given a crack, a vector is created, with the crack length being assigned as the magnitude attribute and the crack orientation as the vector direction, and this vector is referred to as the crack length vector. Crack width and area vectors are defined in a similar way. Additionally, statistical analyses are performed to obtain the angular distributions of the crack length, width, and area vectors.

In the field of the micromechanics of granular materials, the microstructures of granular assemblies are quantified using the fabric tensor (Stake 1982; Kanatani 1984; Rothenburg and Bathurst 1989; Oda 1999; Yang and Dai 2011; Dai et al. 2015; 2016; Dai and Yang 2017; Dai et al. 2017). Within the formulation framework of the fabric tensor, Rothenburg and Bathurst (1989) used several continuous functions to describe the angular distribution of the microstructures and contact force network. Obviously, the methodologies, which are adopted in the field of micromechanics for the characterization of the microstructures and contact force network of granular media, can lend support to a quantitative evaluation of the angular distributions of the vector quantities of cracks put forward in present study. Hence, the related theories and methodologies used in the micromechanics field are used herein for quantitative analyses of the vector data.

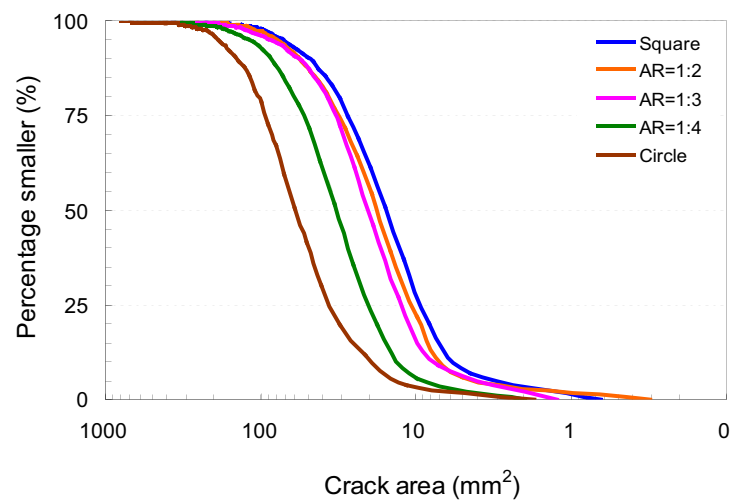
Fig. 6 Cumulative distribution curves of **a** crack lengths, **b** crack widths, and **c** crack areas for various container shapes



(a)

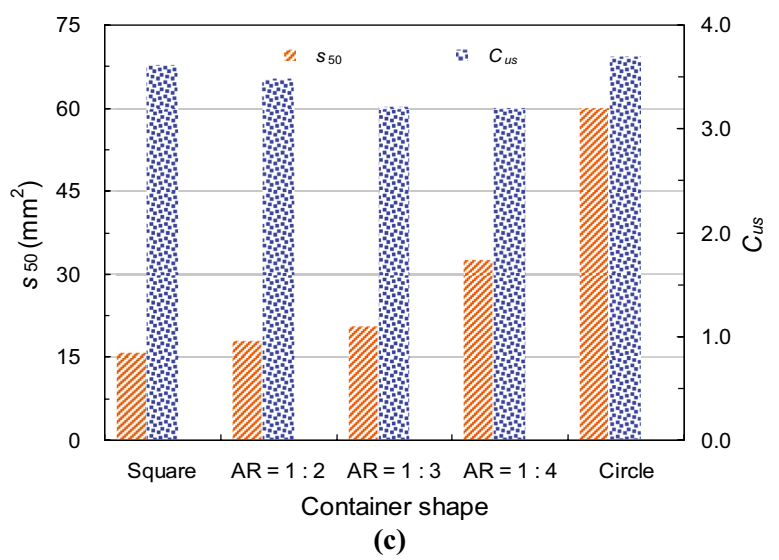
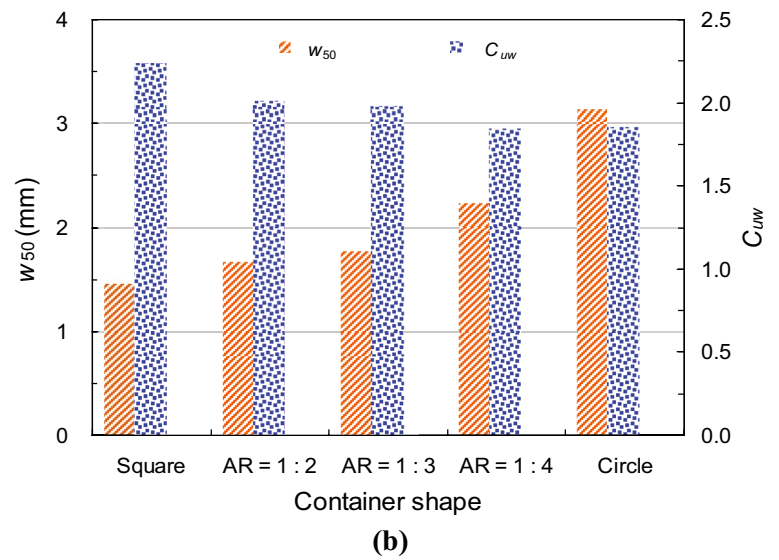
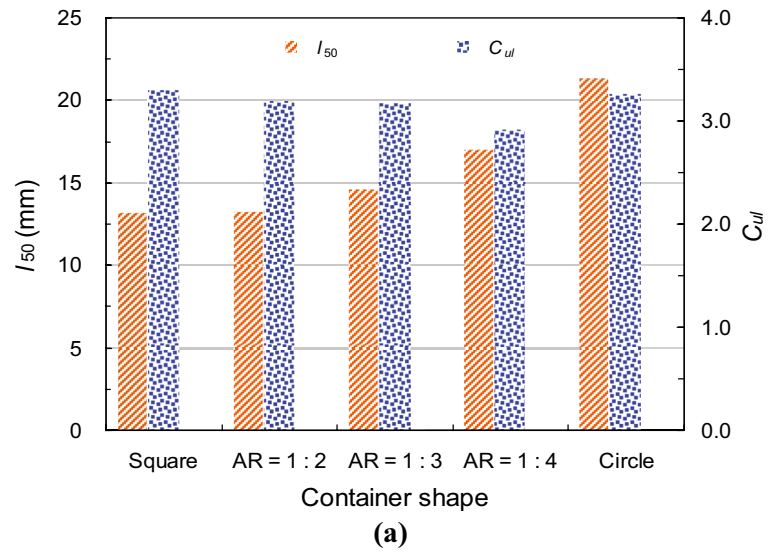


(b)



(c)

Fig. 7 Median values and coefficients of uniformity characterizing the cumulative distribution curves of **a** crack lengths, **b** crack widths, and **c** crack areas for various container shapes



For the characterization of the distribution of cracks in the network, the crack orientation unit vector, as shown in Fig. 5, is used to formulate a fabric tensor. The second-ranked fabric tensor is (Oda 1999)

$$F_{ij} = \frac{1}{2N} \sum_{k=1}^{2N} n_i^k n_j^k \tag{1}$$

where N is the crack number and n_i^k ($i = 1, 2, 3$ in the three-dimensional (3D) case and $i = 1, 2$ in the two-dimensional (2D) case) are the directional cosines of a crack orientation unit vector n^k with reference to the axes in a Cartesian coordinate system (see the 2D Cartesian coordinate system in Fig. 4). With the introduction of a density function $E(n)$, F_{ij} is re-expressed in integral form (Rothenburg and Bathurst 1989) as

$$F_{ij} = \int_{\Omega} E(n) n_i n_j d\Omega \tag{2}$$

where Ω is the representative elemental volume. The density function $E(n)$ is written as

$$E(n) = E_0(1 + d_{ij}n_i n_j) \tag{3}$$

where E_0 is the distribution probability density in an isotropic state and equals $1/(2\pi)$ in the 2D case, d_{ij} is a deviatoric tensor of second rank quantifying the deviation from an isotropic distribution, and the subscripts $i, j = 1, 2$ in the 2D case. The unit vector n_i or n_j in the 2D case is

$$\begin{pmatrix} n_1 \\ n_2 \end{pmatrix} = \begin{pmatrix} \cos \phi \\ \sin \phi \end{pmatrix} \tag{4}$$

where ϕ is the orientation angle of the unit vector with respect to the horizontal axis in the 2D Cartesian coordinate system. Equation (3) is thus rewritten as

$$E(\phi) = E_0(1 + d_{11} \cos^2 \phi + d_{12} \cos \phi \sin \phi + d_{21} \sin \phi \cos \phi + d_{22} \sin^2 \phi) \tag{5}$$

Note that d_{ij} is a deviatoric tensor with the trace being zero; i.e., $d_{11} + d_{22} = 0$. With this condition, Eq. (5) is rewritten as

$$E(\phi) = E_0(1 + d_{11} \cos^2 \phi + 2d_{12} \sin \phi \cos \phi - d_{11} \sin^2 \phi)$$

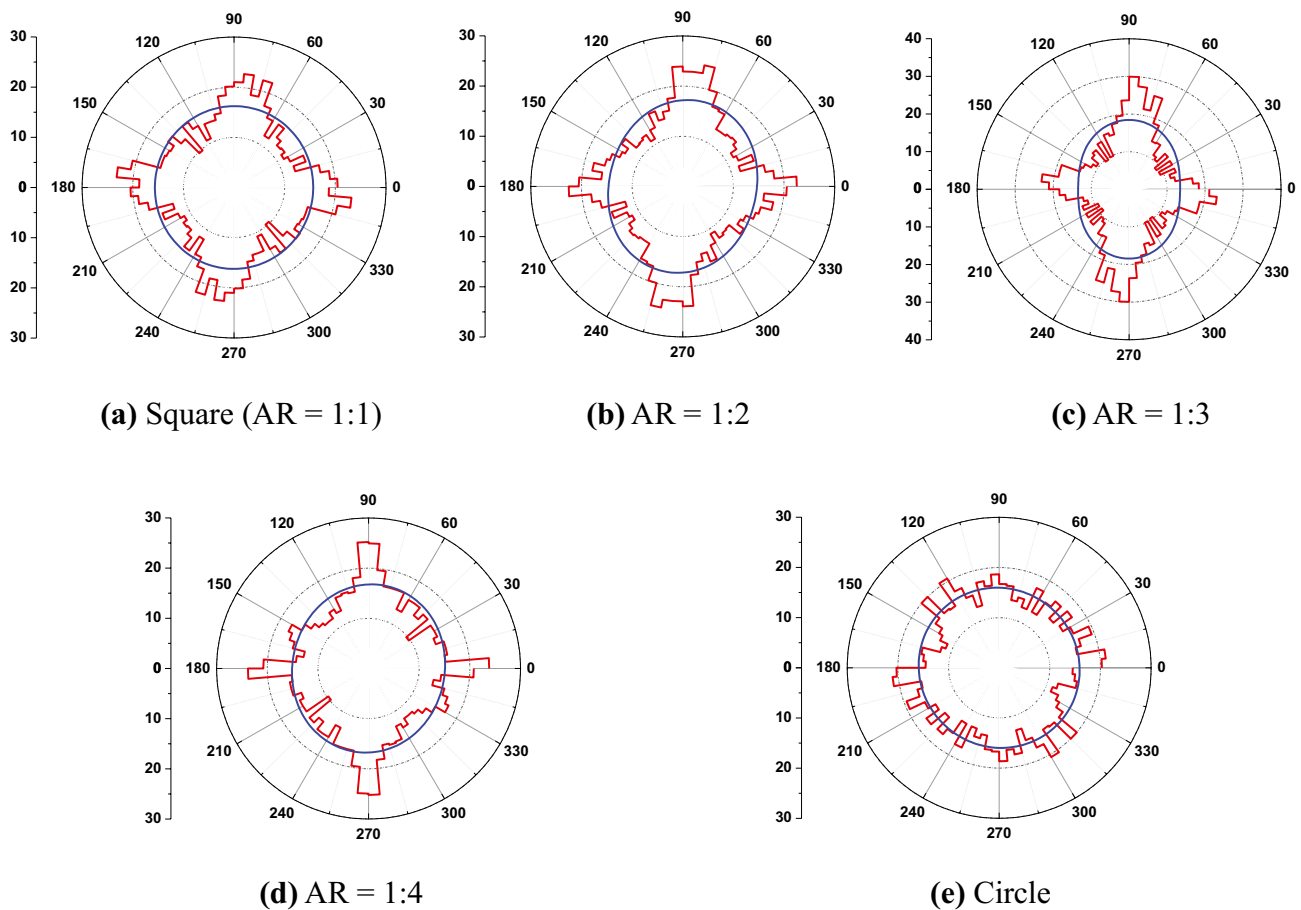


Fig. 8 Probability density (%) of the angular distribution of crack orientation vectors in containers of different shape

$$E(\phi) = E_0(1 + d_{11} \cos 2\phi + d_{12} \sin 2\phi)$$

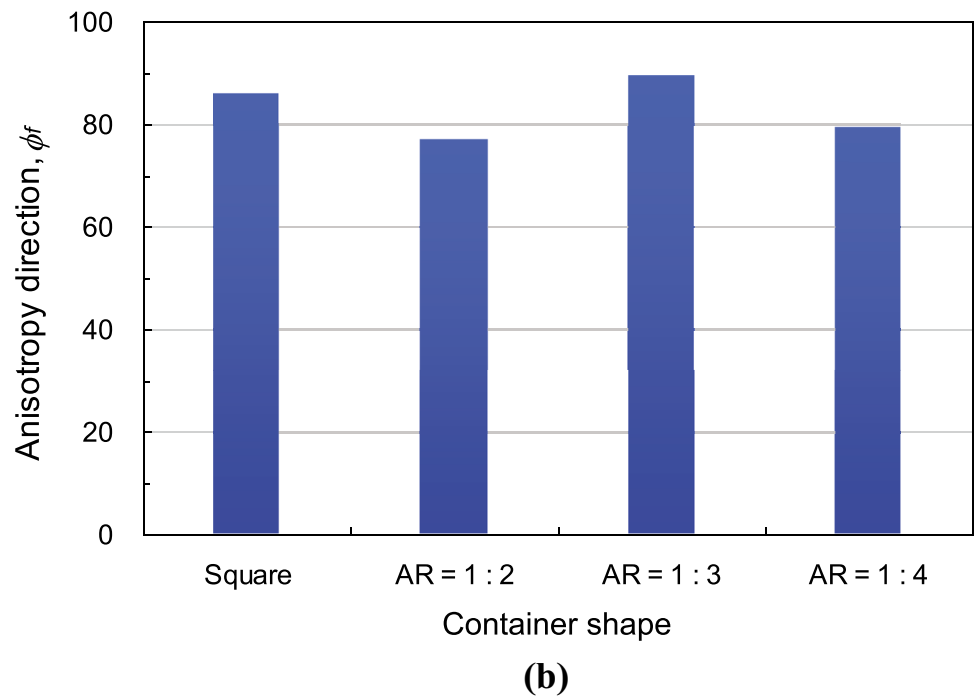
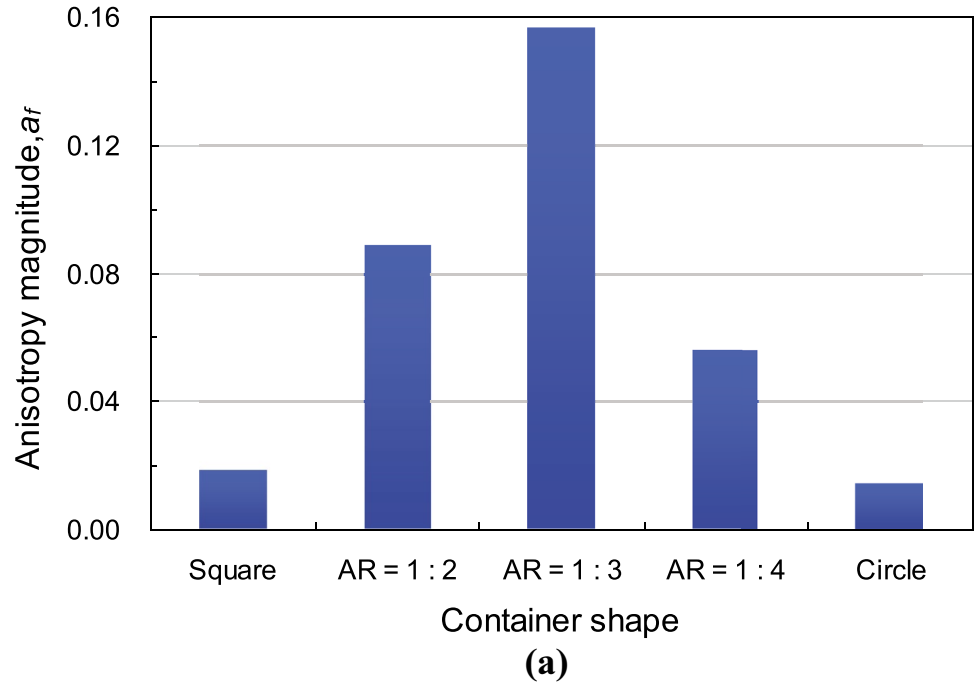
$$E(\phi) = E_0 \left\{ 1 + \sqrt{d_{11}^2 + d_{12}^2} \left(\frac{d_{11}}{\sqrt{d_{11}^2 + d_{12}^2}} \cos 2\phi + \frac{d_{12}}{\sqrt{d_{11}^2 + d_{12}^2}} \sin 2\phi \right) \right\} \quad (6)$$

Hence, $E(\phi)$ is redefined as

$$E(\phi) = E_0 \{ 1 + a_f \cos 2(\phi - \phi_f) \} \quad (7)$$

where a_f is the magnitude of anisotropy and ϕ_f is the principal direction of anisotropy. The function value of $E(\phi)$ in Eq. (7) is interpreted as the distribution probability density

Fig. 9 Comparison of **a** the anisotropy magnitudes and **b** principal directions (°) of anisotropy with regard to the angular distributions of crack orientation vectors in containers of different shape



of crack orientation unit vectors at a given direction specified by the angle ϕ . The parameters a_f and ϕ_f are two essential anisotropy indices obtained by equating Eq. (1) to Eq. (2) as.

$$a_f = \sqrt{d_{11}^2 + d_{12}^2} \quad \text{and} \quad \phi_f = \frac{1}{2} \arctan\left(\frac{d_{12}}{d_{11}}\right) \quad (8)$$

Following the methodology introduced above, three other continuous functions, which are similar to the function in Eq. (7), are introduced to characterize the angular distributions of the crack length, width, and area vectors.

Crack length vector:

$$C(\phi) = C_0 \{1 + a_c \cos 2(\phi - \phi_c)\} \quad (9)$$

Crack width vector:

$$W(\phi) = W_0 \{1 + a_w \cos 2(\phi - \phi_w)\} \quad (10)$$

Crack area vector:

$$M(\phi) = M_0 \{1 + a_m \cos 2(\phi - \phi_m)\} \quad (11)$$

Here, C_0 is a measure of the mean crack length with the cracks in various directions given equal weight, and W_0 and

M_0 are defined similarly to C_0 . a_c , a_w , and a_m are the anisotropy magnitudes for the crack length, width, and area vectors, respectively, and ϕ_c , ϕ_w , and ϕ_m are the corresponding principal directions of anisotropy. For clarity and ease of comparison, the statistical analyses are done with regard to vectors normalized by the mean vector magnitude, such that Eqs. (9)–(10) are rewritten as follows:

Crack length vector:

$$\frac{C(\phi)}{C_0} = 1 + a_c \cos 2(\phi - \phi_c) \quad (12)$$

Crack width vector:

$$\frac{W(\phi)}{W_0} = 1 + a_w \cos 2(\phi - \phi_w) \quad (13)$$

Crack area vector:

$$\frac{M(\phi)}{M_0} = 1 + a_m \cos 2(\phi - \phi_m) \quad (14)$$

Note that the methodology proposed for the anisotropy analysis of the cracking pattern in this study is also applicable to describing the anisotropic properties of cracks generated

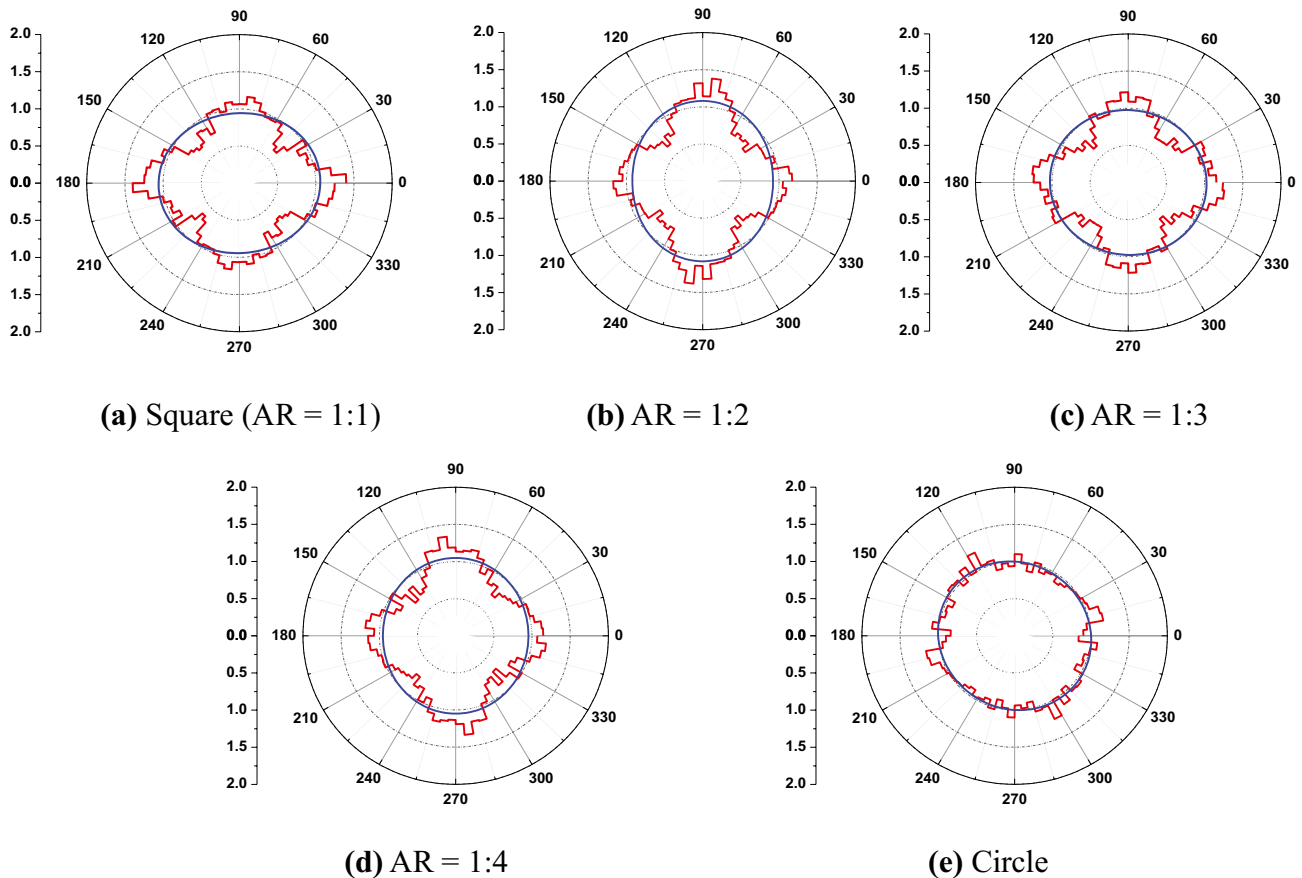
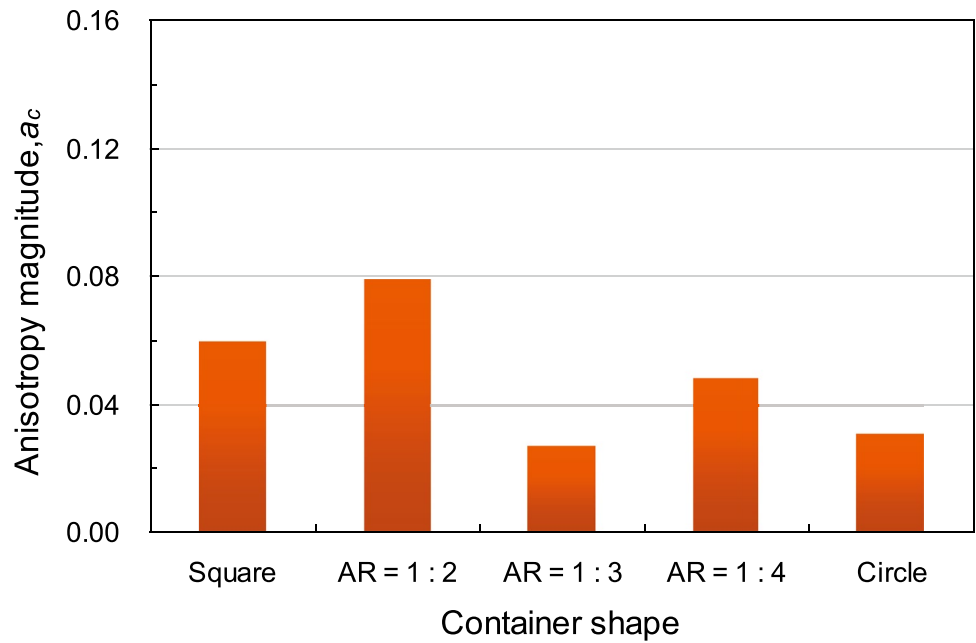
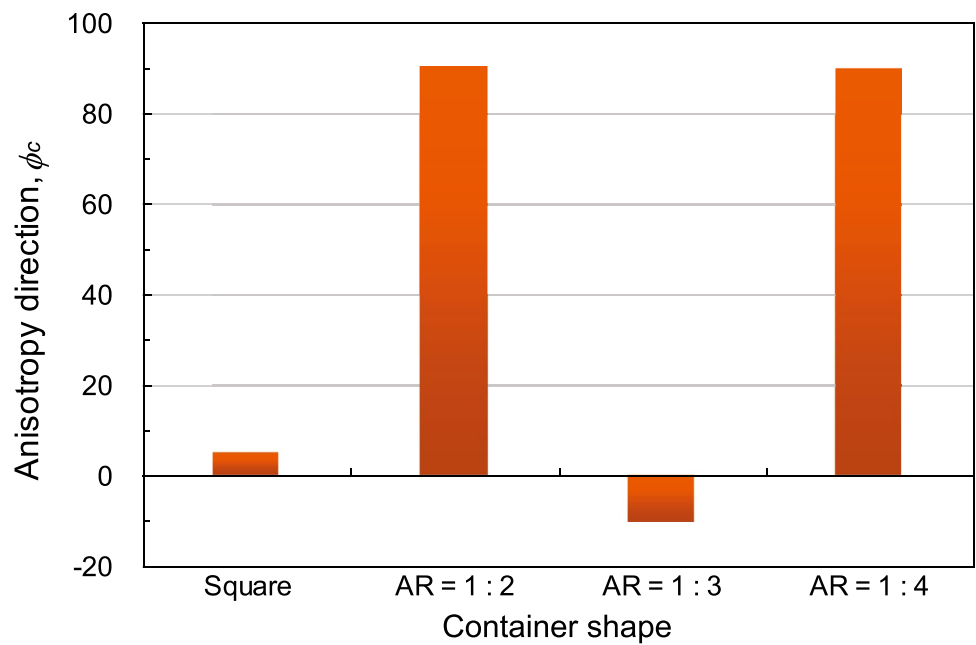


Fig. 10 Angular distributions of the normalized crack length vectors in containers of different shape

Fig. 11 Comparison of **a** the anisotropy magnitudes and **b** principal directions ($^{\circ}$) of anisotropy with regard to the angular distributions of normalized crack length vectors in containers of different shape



(a)



(b)

in other environments, such as the freeze–thaw cycling environment (Lu et al. 2016), in that the anisotropy analysis of the crack network, which involves the characterization and statistics of a number of vector quantities, generally follows the same principle. It is also worth mentioning that the main objectives of the present study are to introduce a methodology

of analyzing the crack distribution anisotropy and to examine the effect of the boundary conditions (i.e., container shape), and the evolution of anisotropy is not the focus of the study. Therefore, the variations in the water content and crack distribution anisotropy were not tracked during the soil desiccation process.

Results and discussions

Crack network analysis with scalar data

Figure 6 presents the cumulative distribution curves of the crack lengths, widths, and areas for the considered container shapes. It is seen that the curves for the square and circular shapes serve as the boundaries, with the curves for other shapes falling between them, regardless of whether such curves are for crack lengths, widths, or areas. It is also interesting that these distribution curves seem to have similar overall shapes. Figure 7 compares the median values and uniformity coefficients for such distribution curves. It is shown that the median values (i.e., l_{50} , w_{50} , and s_{50}) are the largest for the circular shape whereas those for other shapes increase with a decrease in the aspect ratio of the containers; i.e., a smaller AR results in a higher median value. The coefficients of uniformity (i.e., C_{ul} , C_{uw} , and C_{us}) decrease with a decreasing aspect ratio given that the case of the circular shape is not considered, which indicates that the lengths, widths, and areas of the cracks tend to become uniform as the AR decreases. It is also found that C_{uw} (< 2.5) is on average less than C_{ul} and C_{us} (both > 2.5), meaning that the

distribution of the crack widths is more uniform than the distributions of the crack lengths and areas.

Crack network anisotropy analysis with vector data

Crack orientation vector

Figure 8 depicts the angular distributions of crack orientation vectors in the containers having various shapes. The blue closed curves present the approximation made with Eq. (7). It is seen that the angular distributions in the cases of square and rectangular shapes have an obvious feature of orthogonal concentration and the preferred distribution directions of crack orientations lie in two angular regions (i.e., $-15^\circ < \phi < 15^\circ$ and $75^\circ < \phi < 105^\circ$) near the horizontal and vertical directions. That is, the cracks tend to develop around the directions of the container boundaries and the probability of cracks orienting in such two angular regions is higher than that for other regions. Nonetheless, the angular distribution in the case of the circular shape, which has an almost isotropic pattern, does not demonstrate the feature of orthogonal concentration. The occurrence of the

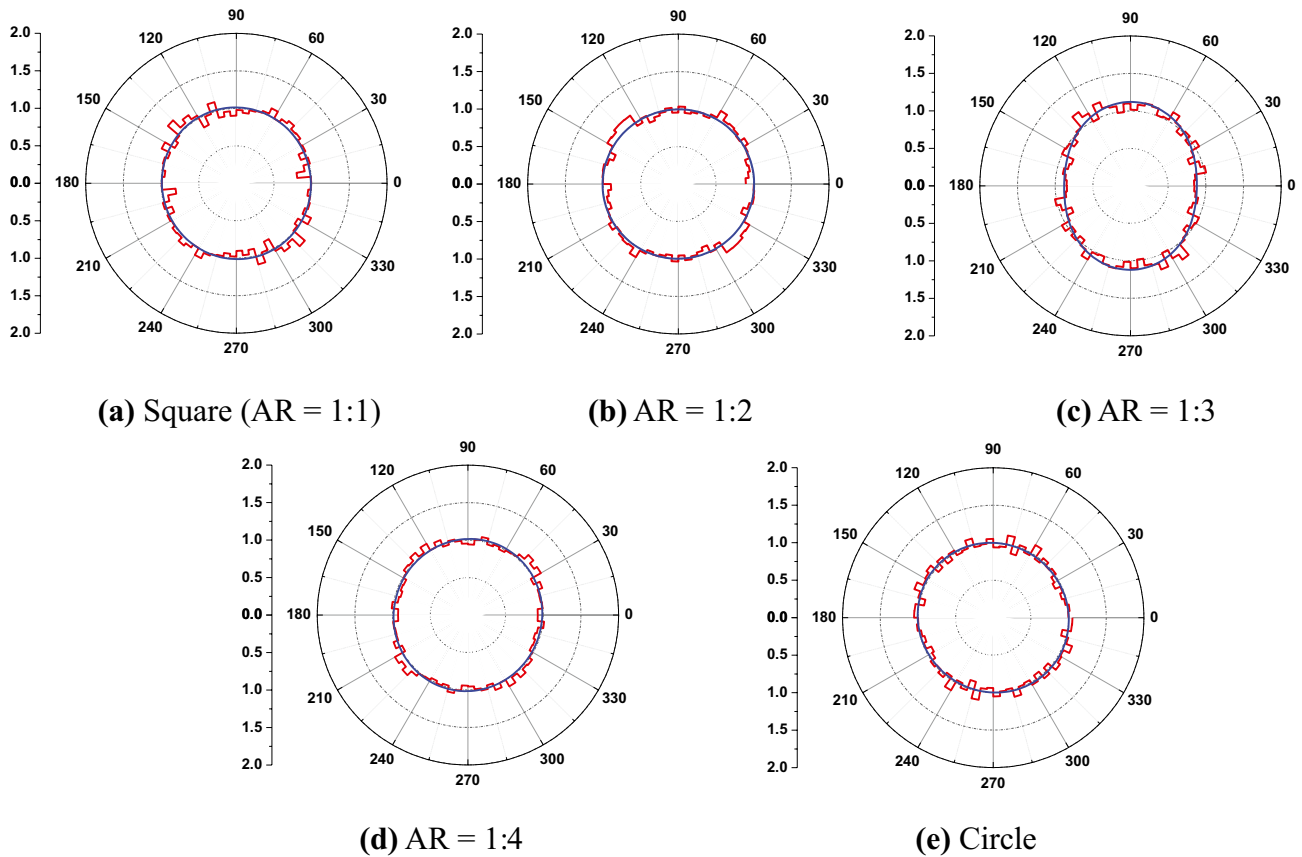


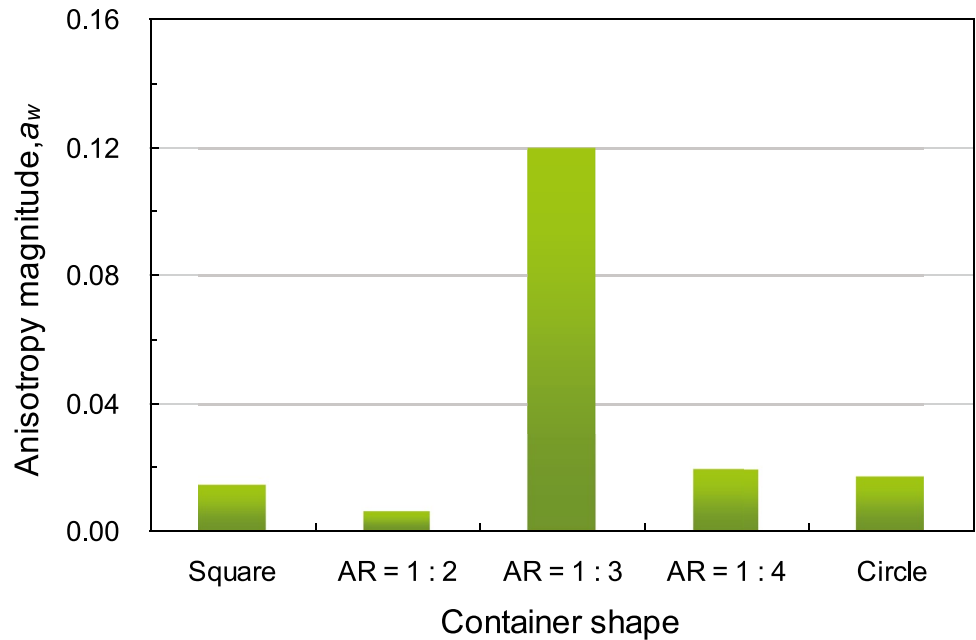
Fig. 12 Angular distributions of normalized crack width vectors in containers of different shape

orthogonal concentration is primarily due to the perpendicular boundaries externally constraining the deformation field of soil layers, making the boundary directions the prevailing directions for the crack development (Wang et al. 2018). It is also inferred that the concentration orthogonality is interrelated with the finding reported in

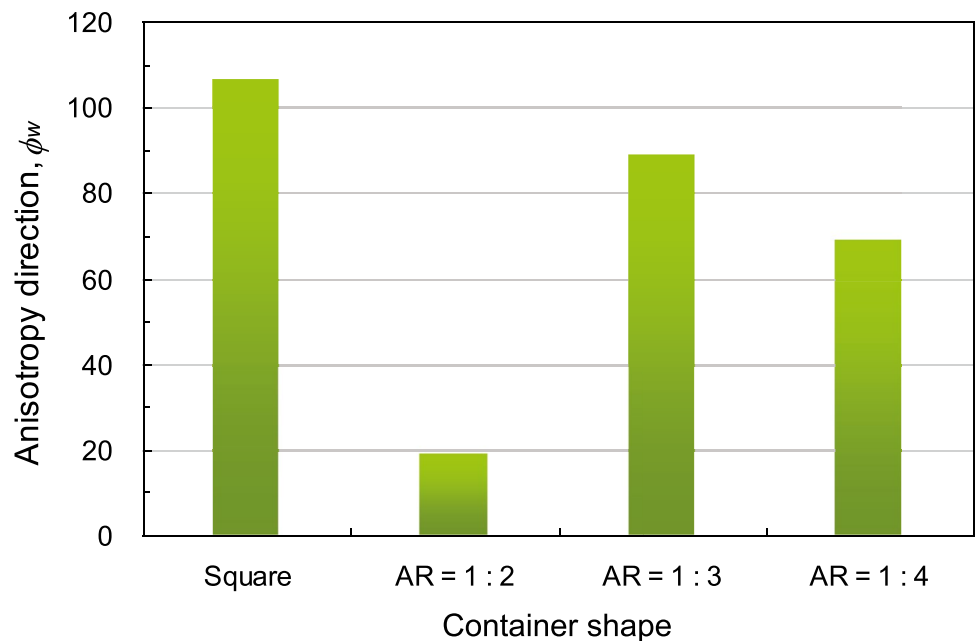
the literature that a secondary crack in general develops in a direction perpendicular to a primary crack.

Figure 9 gives the anisotropy magnitudes and principal directions of anisotropy for the angular distributions in Fig. 8. The case of the circular shape is excluded from the examination of the principal direction of anisotropy because

Fig. 13 Comparison of **a** the anisotropy magnitudes and **b** principal directions (°) of anisotropy with regard to the angular distributions of normalized crack width vectors in containers of different shape



(a)



(b)

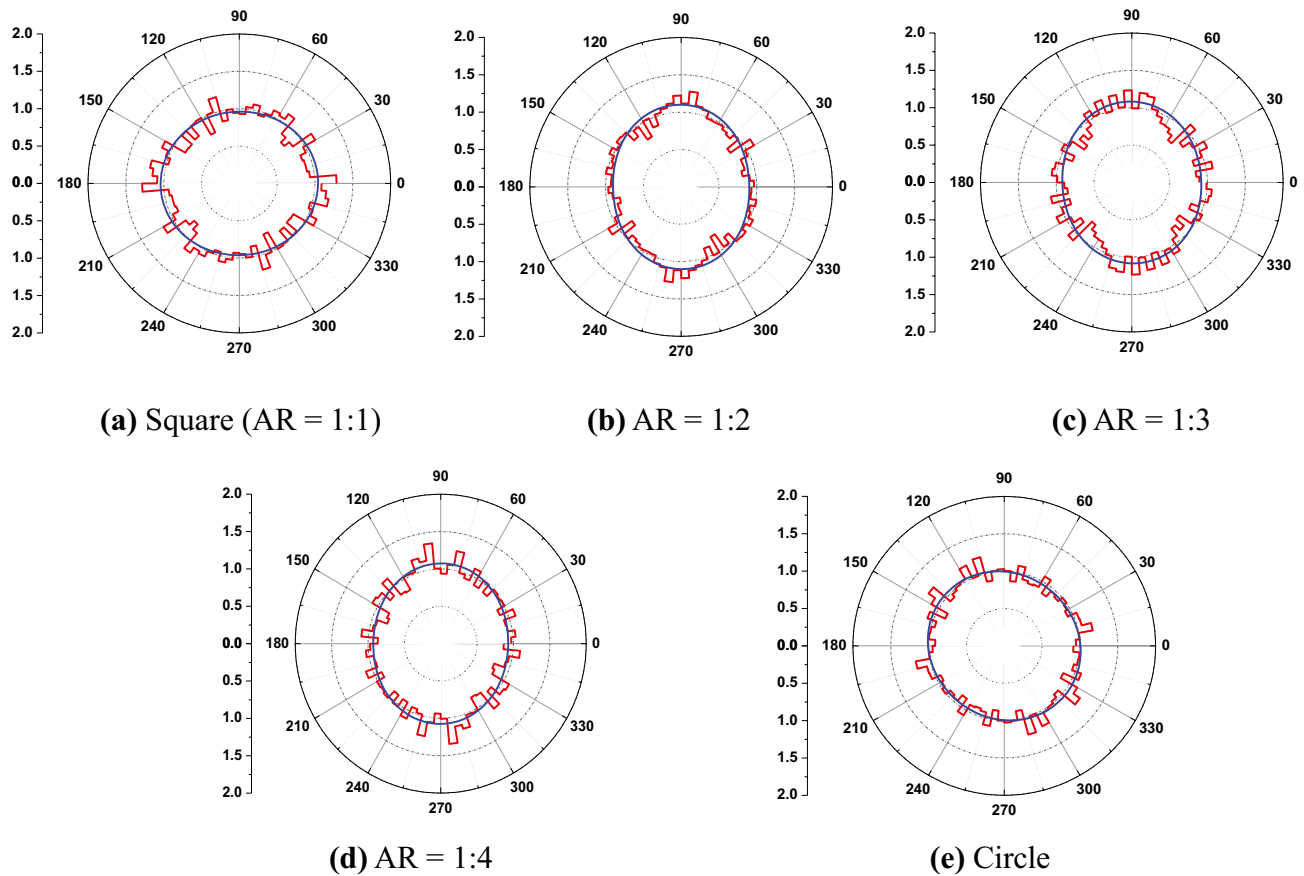


Fig. 14 Angular distributions of normalized crack area vectors in containers of different shape

there exists no particular reference side when conducting the imaging analysis for this shape. It is seen that the anisotropy magnitude ($a_f=0.014$) is the smallest for the circular shape, and this is evidence of an almost isotropic distribution. The anisotropy magnitude ($a_f=0.019$) for the case of a square shape is similarly at a low level, and its principal direction of anisotropy is near vertical. It is noted that a small anisotropy magnitude for the square shape does not refer to an almost isotropic distribution pattern but means that the distribution concentrations around the principal direction of anisotropy (close to the vertical direction) and its orthogonal direction (close to the horizontal direction) are similar to each other. In other words, the probabilities of cracks orienting around the horizontal and vertical directions are basically the same, even though the angular distribution pattern has the feature of orthogonal concentration.

The anisotropy magnitudes for all other rectangular shapes exceed 0.04. The largest value ($a_f=0.157$) is for the case that AR = 1:3, indicating that the angular distribution of crack orientation vectors has weak to moderate anisotropy. It is noted that the principal directions of anisotropy

are adjacent to the vertical direction. These observations suggest that the angular distributions of crack orientations for rectangular shapes have the characteristics of both anisotropy and orthogonal concentration. In view of such a composite feature, it can be stated that the degree of the distribution concentration around the principal direction of anisotropy (near the vertical direction) is higher than that around the orthogonal direction (near the horizontal direction), despite the two orthogonal directions both being preferred directions. Additionally, the degree of the distribution concentration in such cases is higher than that in the case of the square shape. A relatively large anisotropy magnitude generally signifies a relatively high degree of concentration around the principal direction of anisotropy.

Crack length vector

Figure 10 presents rose diagrams characterizing the angular distributions of (normalized) crack length vectors. The blue closed curves present the approximation given by Eq. (12). The rose diagrams in Fig. 10 are, to some extent, similar

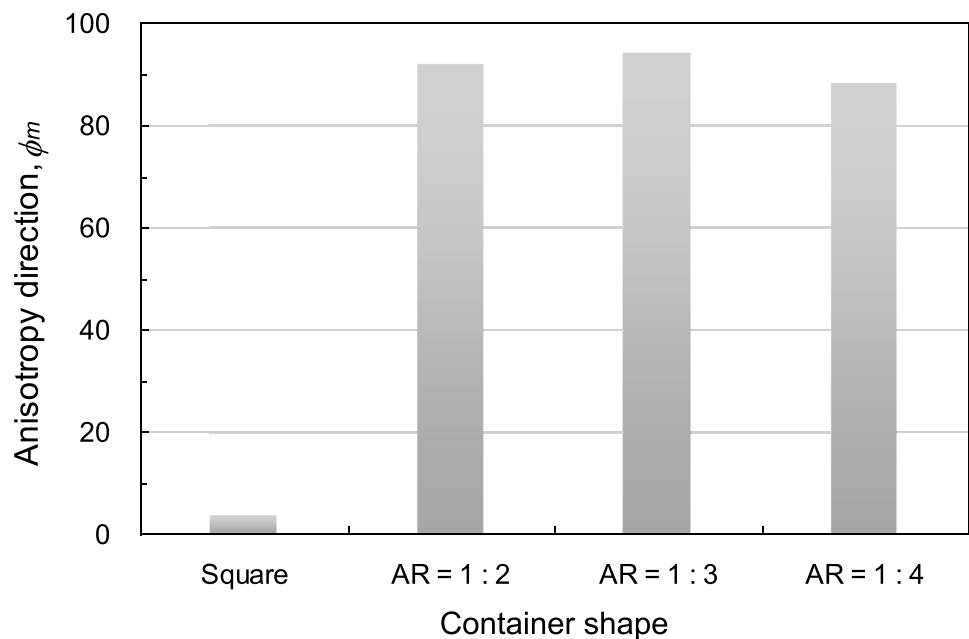
to those in Fig. 8. To be specific, the feature of orthogonal concentration around the horizontal and vertical directions appears in the rose diagrams for the square and rectangular shapes; the angular distribution in the case of the circular shape fails to display the orthogonal concentration and approximates to an almost isotropic form as evidenced by the anisotropy magnitude ($a_c = 0.03$) given in Fig. 11a. Such

observations indicate that for the square and rectangular shapes, the cracks in the angular regions of $-15^\circ < \phi < 15^\circ$ and $75^\circ < \phi < 105^\circ$ are on average longer than those in other regions; i.e., relatively long cracks are prone to develop around the directions of boundaries for a rectangular (or square) container. As regards the case of the circular shape, the crack lengths are basically the same in all directions.

Fig. 15 Comparison of **a** the anisotropy magnitudes and **b** principal directions ($^\circ$) of anisotropy with regard to the angular distributions of normalized crack area vectors in containers of different shape



(a)

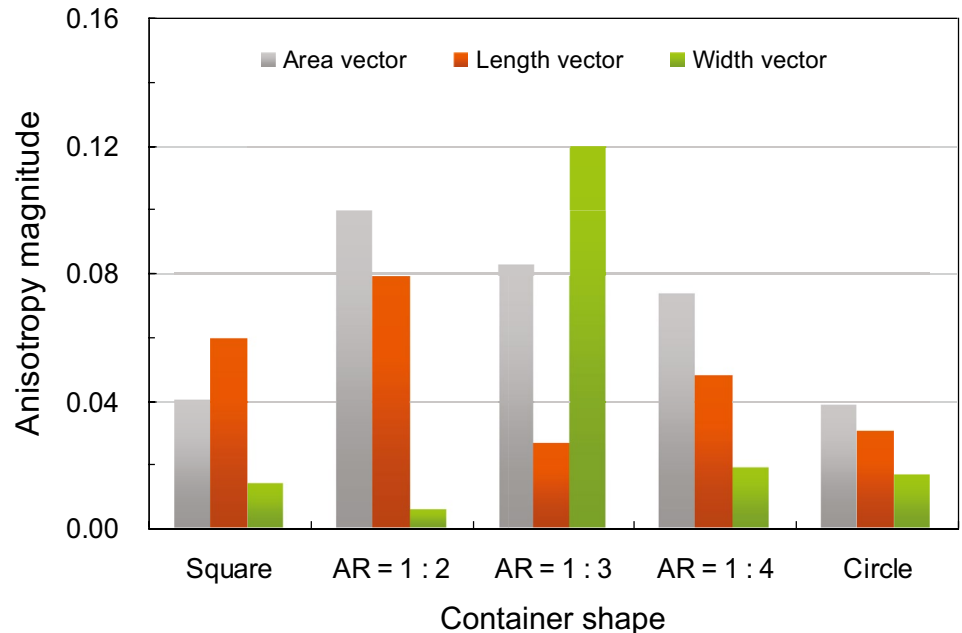


(b)

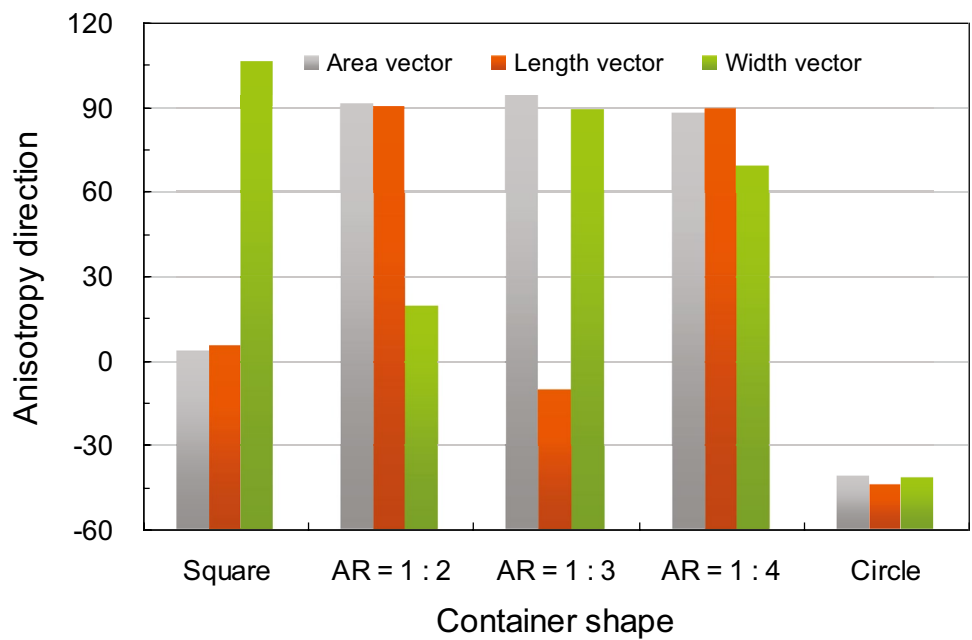
Figure 11a reveals that the anisotropy magnitude ($a_c=0.027$) in the case that $AR=1:3$ is close to that for the circular shape. Nevertheless, such a small value, as clarified above, does not mean an approximation to an isotropic distribution pattern but signifies an almost equivalent concentration degree for the angular distributions of the crack length vectors in the two orthogonal angular regions. The

anisotropy magnitudes for the three other shapes are above 0.04 but less than 0.1, which indicates weak anisotropy. The principal directions of anisotropy, as indicated by Fig. 11b, are near either the horizontal direction or the vertical direction. The low anisotropy magnitude ($0.04 < a_c < 0.1$) suggests that the cracks around the principal direction of anisotropy are a little longer than those around the orthogonal

Fig. 16 Comparison of anisotropy in terms of the angular distributions of normalized crack length, width and area vectors: **a** anisotropy magnitude and **b** principal directions ($^\circ$) of anisotropy



(a)



(b)

direction. It is also concluded that in the rose diagrams, the concentration near the principal anisotropy direction is slightly higher than that near the orthogonal direction.

Crack width vector

Figure 12 presents rose diagrams describing the angular distributions of (normalized) crack width vectors. Aside from the case that $AR = 1:3$, the angular distributions are seen to have an approximately isotropic pattern, and the anisotropy magnitudes, as indicated in Fig. 13a, are at a low level ($a_w < 0.04$), meaning that the angular distributions of crack width vectors do not exhibit any concentration around a certain preferred direction. It is also implied that the cracks, on average, have almost the same width in different angular directions. The angular distribution has a moderate anisotropic form in the case that $AR = 1:3$, with the anisotropy magnitude a_w being 0.12 and the principal direction of anisotropy being around the vertical direction (see Fig. 13a, b). This signifies that the crack widths near the principal anisotropy direction (beside the vertical direction) are on average the largest.

Crack area vector

Figure 14 describes with rose diagrams the angular distributions of (normalized) crack area vectors. It is clear that none of rose diagrams exhibit the orthogonal concentration. The angular distributions for both square and circular shapes demonstrate a lower degree of anisotropy as compared with the other three cases, and they can be considered to have a nearly isotropic pattern, with their anisotropy magnitudes, as evidenced by Fig. 15a, being less than 0.04. The angular distributions of the crack area vectors for the other three rectangular shapes are observed to have a pattern of weak anisotropy. Figure 15 shows that their anisotropy magnitudes range between 0.04 and 0.1 and the principal directions of anisotropy are near the vertical direction. It is concluded that the crack area around the principal anisotropy direction is relatively large and that around the orthogonal direction is comparatively small.

The area of a crack is obtained as a product of its length and width. It is thus reasonable to infer that the distribution anisotropy of crack area vectors depends on the distribution anisotropy of the crack length and width vectors. For a close examination, Fig. 16 makes an overall comparison of the anisotropy magnitudes and principal directions of anisotropy, which are derived from the angular distributions of crack length, width, and area vectors. It is found that given a particular container shape, the anisotropy magnitude of the crack area vector approximates more to a relatively large anisotropy magnitude value that is for either the crack length or width vector, and the principal direction of anisotropy is

closer to the direction associated with the vector having a relatively large anisotropy magnitude. It can therefore be said that although the crack area is determined by the factors of the length and width, the distribution anisotropy of crack area vectors is more affected by the vector (i.e., either the crack length or width vector), the angular distribution of which bears stronger anisotropy.

Summary

A series of desiccation cracking tests were carried out with respect to thin soil layers in containers with various boundary shapes. A statistical analysis of the crack network morphology was conducted by focusing on the distributions of scalar and vector quantities obtained through image analyses using the software CIAS. Efforts were made to gain insights from the perspective of the distribution anisotropy of vector quantities. The main findings of the study are summarized as follows.

- (a) The median values of the crack length, width, and area are all the largest for the circular shape among the considered container shapes. For the square and rectangular shapes, the median values for the crack length, width, and area increase with a decreasing aspect ratio of the containers, and the coefficients of uniformity decrease correspondingly.
- (b) The angular distributions of the crack orientation and length vectors have an approximately isotropic form for the circular shape and the feature of orthogonal concentration in two angular regions around the horizontal and vertical directions (i.e., $-15^\circ < \phi < 15^\circ$ and $75^\circ < \phi < 105^\circ$) for the other container shapes, indicating that the probability of cracks orienting around the directions of boundaries is higher and the crack length around the two perpendicular boundary directions is on the average greater. The occurrence of the orthogonal concentration is mainly attributed to the perpendicular boundaries serving as external constraints of the deformation field of soil layers, making the boundary directions the prevailing directions for the crack initiation and propagation. The orthogonality of the concentration is an overall indicator of secondary cracks developing in directions perpendicular to primary cracks.
- (c) In the case of the square shape, the anisotropy magnitude of crack orientation vectors is small and far less than the anisotropy magnitudes for the rectangular shapes. Concerning the angular distributions of crack orientation and length vectors for the considered shapes other than the circular shape, a small anisotropy magnitude signifies an almost equivalent degree of distribution concentration within the two angular regions

whereas an unignorable anisotropy magnitude means that there is a predominant concentration around the principal direction of anisotropy. A larger magnitude of anisotropy results in a higher degree of concentration around the principal anisotropy direction.

- (d) Apart from the case that $AR = 1:3$, the angular distributions of crack width vectors basically have an isotropic pattern and do not show any concentrations around a certain preferred direction. The angular distribution in the case that $AR = 1:3$ has a moderate anisotropic form.
- (e) The angular distributions of crack area vectors are almost isotropic in the cases of square and circular shapes, whereas those for other rectangular shapes demonstrate weak anisotropy, with the principal directions of anisotropy being near the vertical direction. In particular, the vector (i.e., either the crack length or width vector), the distribution of which has relatively strong anisotropy, dominates the effect on the distribution anisotropy of the crack area vectors.

Acknowledgements The authors appreciate financial support provided by the National Natural Science Foundation of China (No. 52078507), the Science and Technology Program of Guangzhou City under grant No. 202002030195, the Science and Technology Program of Zhuhai City under grant No. ZH22036204200009PWC, and the Natural Science Foundation of Guangdong Province under grant No. (2018A030313897). Support from HKRGC under the General Research Fund scheme (Grant No. 17250316) is also acknowledged. The authors extend their sincere gratitude to Mr. Chang-Wen Xu and Mr. Yi-Yuan Chen for their kind assistance in the experimental work.

References

- Akiba Y, Shima H (2019) Flow-velocity-dependent transition of anisotropic crack patterns in CaCO_3 paste. *J Phys Soc Jpn* 88:024001
- Alava MJ, Nukala PKVV, Zapperi S (2006) Morphology of two dimensional fracture surfaces. *J Stat Mech* 10:L10002
- An N, Tang C, Cheng Q, Wang D, Shi B (2020) Application of electrical resistivity method in the characterization of 2D desiccation cracking process of clayey soil. *Eng Geol* 265:105416
- Arena A, Delle Piane C, Sarout J (2014) A new computational approach to cracks quantification from 2D image analysis: application to micro-cracks description in rocks. *Comput Geosci* 66:106–120
- Bai T, Pollard DD, Gao H (2000) Explanation for fracture spacing in layered materials. *Nature* 403:753–756
- Baker R (1981) Tensile strength, tension cracks, and stability of slopes. *Soils Found* 21:1–17
- Basson MS, Ayothiraman R (2020) Effect of human hair fiber reinforcement on shrinkage cracking potential of expansive clay. *Bull Eng Geol Environ* 79:2159–2168
- Boehm-Courjault E, Barbotin S, Leemann A, Scrivener K (2020) Microstructure, crystallinity and composition of alkali-silica reaction products in concrete determined by transmission electron microscopy. *Cem Concr Res* 130:105988
- Bohn S, Pauchard L, Couder Y (2005a) Hierarchical crack pattern as formed by successive domain divisions. I. Temporal and geometrical hierarchy. *Phys Rev E* 71:046214
- Bohn S, Platkiewicz J, Andreotti B, Adda-Bedia M, Couder Y (2005b) Hierarchical crack pattern as formed by successive domain divisions. II. From disordered to deterministic behavior. *Phys Rev E* 71:046215
- Bulolo S, Leong EC, Kizza R (2021) Tensile strength of unsaturated coarse and fine-grained soils. *Bull Eng Geol Environ* 80:2727–2750
- Cheng Q, Tang CS, Zhu C, Li K, Shi B (2020) Drying-induced soil shrinkage and desiccation cracking monitoring with distributed optical fiber sensing technique. *Bull Eng Geol Environ* 79:3959–3970
- Cortet P, Huillard G, Vanel L, Ciliberto S (2008) Attractive and repulsive cracks in a heterogeneous. *J Stat Mech* 10:P10022
- Costa S, Kodikara J, Shannon B (2013) Salient factors controlling desiccation cracking of clay in laboratory experiments. *Géotechnique* 63:18–29
- Dai BB, Yang J (2017) Shear strength of assemblies of frictionless particles. *International Journal of Geomechanics ASCE* 17:04017102
- Dai BB, Yang J, Luo XD (2015) A numerical analysis of the shear behavior of granular soil with fines. *Particuology* 21:160–172
- Dai BB, Yang J, Zhou CY (2017) Micromechanical origin of angle of repose in granular materials. *Granul Matter* 19:24
- Dai BB, Yang J, Zhou CY, Luo XD (2016) DEM investigation on the effect of sample preparation on the shear behavior of granular soil. *Particuology* 25:111–121
- DeCarlo KF, Shokri N (2014) Effects of substrate on cracking patterns and dynamics in desiccating clay layers. *Water Resour Res* 50:3039–3051
- Fernandes M, Denis A, Fabre R, Lataste JF, Chrétien M (2015) In situ study of the shrinkage-swelling of a clay soil over several cycles of drought-rewetting. *Eng Geol* 192:63–75
- Goehring L (2013) Evolving fracture patterns: columnar joints, mud cracks and polygonal terrain. *Phil Trans R Soc A* 371:20120353
- Goehring L, Conroy R, Akhter A (2010) Evolution of mud-crack patterns during repeated drying cycles. *Soft Matter* 6:3562–3567
- Gui Y, Zhao GF (2015) Modelling of laboratory soil desiccation cracking using DLSSM with a two-phase bond model. *Comput Geotech* 69:578–587
- Hawkins AB (2013) Some engineering geological effects of drought: examples from the UK. *Bull Eng Geol Environ* 72:37–59
- Hu T, Guilleminot J, Dolbow JE (2020) A phase-field model of fracture with frictionless contact and random fracture properties: application to thin-film fracture and soil desiccation. *Comput Methods Appl Mech Engrg* 368:113106
- Julina M, Thyagaraj T (2020) Combined effects of wet-dry cycles and interacting fluid on desiccation cracks and hydraulic conductivity of compacted clay. *Eng Geol* 267:105505
- Kanatani K (1984) Distribution of directional data and fabric tensors. *Int J Engng Sci* 22:149–164
- Khan MS, Hossain S, Ahmed A, Faysal M (2017) Investigation of a shallow slope failure on expansive clay in Texas. *Eng Geol* 219:118–129
- Khatun T, Dutta T, Tarafdar S (2013) Crack formation under an electric field in droplets of laponite gel: memory effect and scaling relations. *Langmuir* 29:15535–15542
- Khatun T, Dutta T, Tarafdar S (2015) Topology of desiccation crack patterns in clay and invariance of crack interface area with thickness. *Eur Phys J E* 38:83
- Kindle EM (1917) Some factor affecting the development of mud-cracks. *J Geol* 25:135–144
- Kitsunozaki S, Nakahara A, Matsuo Y (2016) Shaking-induced stress anisotropy in the memory effect of paste. *EPL* 114:64002
- Kitsunozaki S, Sasaki A, Nishimoto A, Mizuguchi T, Matsuo Y, Nakahara A (2017) Memory effect and anisotropy of particle arrangements in granular paste. *Eur Phys J E* 40:88
- Kokkonen R, Ovaska M, Laurson L, Alava MJ (2017) Intermittent crack growth in fatigue. *J Stat Mech* 07:073401

- Krisdani H, Rahardjo H, Leong EC (2008) Effects of different drying rates on shrinkage characteristics of a residual soil and soil mixtures. *Eng Geol* 102:31–37
- Lakshminantha MR, Prat PC, Ledesma A (2018) Boundary effects in the desiccation of soil layers with controlled environmental conditions. *Geotech Test J* 41:675–697
- Li JH, Zhang LM (2011) Study of desiccation crack initiation and development at ground surface. *Eng Geol* 123:347–358
- Liu C, Tang CS, Shi B, Suo WB (2013) Automatic quantification of crack patterns by image processing. *Comput Geosci* 57:77–80
- Liu T, Luo H, Ma J, Xie W, Wang Y, Jing G (2016) Surface roughness induced cracks of the deposition film from drying colloidal suspension. *Eur Phys J E* 39:24
- Lu Y, Liu S, Weng L, Wang L, Li Z, Xu L (2016) Fractal analysis of cracking in a clayey soil under freeze-thaw cycles. *Eng Geol* 208:93–99
- Matsuo Y, Nakahara A (2012) Effect of interaction on the formation of memories in paste. *J Phys Soc Jpn* 81:024801
- Miller CJ, Mi H, Yesiller N (1998) Experimental analysis of desiccation cracking propagation in clay liners. *J Am Water Resour Assoc* 34:677–686
- Modes CD, Magnasco MO, Katifori E (2016) Extracting hidden hierarchies in 3D distribution networks *Phys Rev X* 6:031009
- Nakahara A, Matsuo Y (2006a) Imprinting memory into paste to control crack formation in drying process. *J Stat Mech* 07:P07016
- Nakahara A, Matsuo Y (2006b) Transition in the pattern of cracks resulting from memory effects in paste. *Phys Rev E* 74:045102
- Nakayama H, Matsuo Y, Takeshi O, Nakahara A (2013) Position control of desiccation cracks by memory effect and Faraday wave. *Eur Phys J E* 36:1
- Nakahara A, Hiraoka T, Hayashi R, Matsuo Y, Kitsunezaki S (2019) Mechanism of memory effect of paste which dominates desiccation crack patterns. *Phil Trans R Soc A* 377:20170395
- Nishiuma S, Miyazima S (1999) Crack growth and percolation in anisotropically rolled thin plate. *Physica A* 266:209–213
- Oda M (1999) Introduction to mechanics of granular materials ed M Oda and K Iwashita (Publisher: A.A. Balkema Rotterdam Netherlands) 27–35
- Omid GH, Thomas JC, Brown KW (1996) Effect of desiccation cracking on the hydraulic conductivity of a compacted clay liner. *Water Air Soil Pollut* 89:91–103
- Peng X, Zhang Z, Gan L, Yoshida S (2016) Linking soil shrinkage behavior and cracking in two paddy soils as affected by wetting and drying cycles. *Soil Sci Soc Am J* 80:1145–1156
- Péron H, Hueckel T, Laloui L, Hu L (2009) Fundamentals of desiccation cracking of fine-grained soils: experimental characterisation and mechanisms identification. *Can Geotech J* 46:1177–1201
- Rodríguez R, Sánchez M, Ledesma A, Lloret A (2007) Experimental and numerical analysis of desiccation of a mining waste. *Can Geotech J* 44:644–658
- Rothenburg L, Bathurst RJ (1989) Analytical study of induced anisotropy in idealized granular materials. *Géotechnique* 39(1989):601–614
- Sánchez M, Manzoli OL, Guimarães LJN (2014) Modeling 3-D desiccation soil crack networks using a mesh fragmentation technique. *Comput Geotech* 62:27–39
- Satake M (1982) Fabric tensor in granular materials IUTAM Symp. on Deformation and Failure of Granular Materials Delft. 63–68
- Stirling RA (2014) Multiphase modelling of desiccation cracking in compacted cracking in compacted soil. PhD thesis Newcastle University
- Sun WJ, Cui YJ (2017) Investigating the microstructure changes for silty soil during drying. *Géotechnique* 68:1–4
- Tang C, Shi B, Liu C, Zhao L, Wang B (2008) Influencing factors of geometrical structure of surface shrinkage cracks in clayey soils. *Eng Geol* 101:204–217
- Tang C, Shi B, Liu C, Suo WB, Gao L (2011) Experimental characterization of shrinkage and desiccation cracking in thin clay layer. *Appl Clay Sci* 52:69–77
- Tang C, Wang D, Zhu C, Zhou QY, Xu SK, Shi B (2018) Characterizing drying induced clayey soil desiccation cracking process using electrical resistivity method. *Appl Clay Sci* 152:101–112
- Tang C, Zhu C, Leng T, Shi B, Cheng Q, Zeng H (2019) Three-dimensional characterization of desiccation cracking behavior of compacted clayey soil using X-ray computed tomography. *Eng Geol* 255:1–10
- Tay YY, Stewart DI, Cousens TW (2001) Shrinkage and desiccation cracking in bentonite–sand landfill liners. *Eng Geol* 60:263–274
- Tollenaar RN, van Paassen LA, Jommi C (2017) Observations on the desiccation and cracking of clay layers. *Eng Geol* 230:23–31
- Vo TD, Pouya A, Hemmati S, Tang AM (2019) Modelling desiccation crack geometry evolution in clayey soils by analytical and numerical approaches. *Can Geotech J* 56:720–729
- Wang C, Zhang Z, Liu Y, Fan S (2017) Geometric and fractal analysis of dynamic cracking patterns subjected to wetting-drying cycles. *Soil till Res* 170:1–13
- Wang LL, Tang CS, Shi B, Cui YJ, Zhang GQ, Hilary I (2018) Nucleation and propagation mechanisms of soil desiccation cracks. *Eng Geol* 238:27–35
- Weinberger R (1999) Initiation and growth of cracks during desiccation of stratified muddy soils. *J Struct Geol* 21:379–386
- Yang J, Dai BB (2011) Is the quasi-steady state a real behaviour? A micromechanical perspective. *Géotechnique* 61:175–184
- Yuan S, Yang B, Liu J, Cao B (2021) Influence of fibers on desiccation cracks in sodic soil. *Bull Eng Geol Environ* 80:3207–3216
- Zeng H, Tang C, Cheng Q, Inyang HI, Rong DZ, Lin L, Shi B (2019) Coupling effects of interfacial friction and layer thickness on soil desiccation cracking behavior. *Eng Geol* 260:105220
- Zhang Y, Ye WM, Chen B, Chen YG, Ye B (2016) Desiccation of NaCl-contaminated soil of earthen heritages in the Site of Yar City, northwest China. *Appl Clay Sci* 124–125:1–10
- Zhang Z, Zhu W, Zhu C, Wang C, Wu C, Si H (2013) Statistical characteristics of random distribution of shrinkage cracks on farmland soil surface. *Trans Chin Soc Agric Eng* 29:119–124
- Zhao YP, Chen J, Yuan Q, Cheng C (2016) Microcrack connectivity in rocks: a real-space renormalization group approach for 3D anisotropic bond percolation. *J Stat Mech* 01:013205